Journal of Sound and Vibration (2000) **237**(1), 81–100
doi:10.1006/jsvi.2000.3056, available online at http://www.idealibrary.com on IDEAL®

HYBRID NOISE CONTROL IN DUCTS

THEODORE M. KOSTEK AND MATTHEW A. FRANCHEK

School of Mechanical Engineering, Purdue University, 1077 Ray W. Herrick Labs., West Lafayette, IN 47907-1077, U.S.A.

(*Received* 1 *March* 1999, *and in final form* 24 *March* 2000)

Presented in this paper is a hybrid noise control system used to attenuate multi-tonal noise in ducts. The hybrid system is built by integrating active feedback noise control with adaptive–passive noise control. The adaptive–passive part of the hybrid noise control system attenuates the dominant tonal noise within the duct while the active noise control system attenuates the noise at other frequencies. To achieve such a hybrid system, the constituent technology for each noise control solution is extended. In particular, an algorithm is described for tuning adaptive–passive noise control devices in the presence of multi-tone noise sources. Also, a feedback controller design methodology is presented. This methodology, adapted from the robust control literature, is easily applied to uncertain acoustic duct systems possessing significant time delays. In the system studied, the time delay arises from the non-collocation of the microphone and the control speaker. The uncertain dynamics of the duct are due to the on-line tuning of the adaptive–passive element. The extended adaptive–passive and robust noise control technologies are combined into a hybrid system. Experimental results are included as are extensions to broadband noise sources.

1. INTRODUCTION

The two basic classifications of low-frequency noise control solutions are passive and active. Each classification has unique advantages and disadvantages leading to a series of performance trade-offs during implementation. This investigation seeks to integrate passive and active solutions to minimize the performance trade-offs. To motivate the proposed hybrid noise control system, an overview of passive noise control solutions will be presented in this section followed by a summary of active feedback noise control studies.

The sidebranch Helmholtz resonator is one passive solution applied to low-frequency duct noise control. An appropriately tuned Helmholtz resonator can achieve sound pressure level reductions of 20 dB or more in realistic applications [1, 2]. The primary limitation of Helmholtz resonators is that sound pressure level reduction is achieved only over a narrow frequency band near the natural frequency of the resonator. The noise attenuation band can be broadened by introducing damping within the Helmholtz resonator. However, this broadening comes at the expense of noise attenuation performance.

Bernhard [3] discusses a way to extend Helmholtz resonators using "adaptive–passive" technology. Adaptive–passive technology offers one way to mitigate the performance trade-offs associated with Helmholtz resonators and improve robustness to variations in the frequency of the tone. It has been shown that a self-tuning, or adaptive–passive, Helmholtz resonator has significantly better sound pressure level attenuation than a fixed resonator in the presence of time-varying tonal disturbances [4]. While several workers have shown the benefits of adaptive–passive devices [5, 6], only a few investigators have

0022-460X/00/410081 + 20 $35.00/0

explicitly developed tuning algorithms [1, 4, 7]. Furthermore, the algorithms which have been developed are incapable of tuning in the presence of multiple tones or broadband noise. Instead, each solution is based on the assumption that the noise spectrum is dominated by a single tone. To use adaptive–passive systems in the presence of multi-tonal noise, therefore, a new tuning algorithm must be developed.

The second class of low-frequency noise control, active noise control, does not suffer from the narrow bandwidth restrictions characteristic of Helmholtz resonators. Recent efforts in active noise control (ANC) can be separated into either adaptive feedforward control or robust feedback control. Although each ANC approach has unique advantages and disadvantages over the other, only feedback-based ANC solutions will be considered in this study. The primary reasons for limiting the ANC to a fixed-filter feedback-based solution include robust stability issues, implementation issues, and the elimination of a second microphone.

One feedback-based ANC scheme that is well known in the literature is the so-called tight-coupled monopole. Trinder and Nelson [8] showed that a high degree of noise attenuation can be achieved at the resonant frequencies within a duct using a tight-coupled monopole. However, the microphone and loudspeaker are required to be collocated to minimize the time delay between the sensor and the secondary source. In general, time delays within feedback loops have a destabilizing effect. Therefore, the elimination of the time delays within feedback systems is attractive. Hong *et al.* [9] studied both single and double (tandem) tight-coupled monopoles. As in the study by Trinder and Nelson [8], the feedback controller was realized by an inverting amplifier and the design process consisted of tuning the amplifier gain such that the closed-loop system was on the verge of instability. This feedback system required a low-pass filter and acoustic damping material to achieve stability.

The feedback controller design methodology espoused in these studies imposes unnecessary constraints on the system performance. These studies seek to achieve maximum noise attenuation at the cost of vanishing stability margins. Such low stability margins limit the application of tight-coupled monopoles. Another shortcoming is that the performance of the closed-loop system is adjusted at all frequencies simultaneously. Consequently, to avoid destabilizing the higher resonances or non-propagating modes, acoustic damping material must be added to the duct or additional low-pass filters must be added to the feedback system. Finally, a system with significant uncertainty would be difficult to stabilize. To realize the full potential of a feedback ANC system, a more flexible design methodology than the typical tight-coupled monopole system must be developed.

Given a methodology to design feedback controllers for uncertain acoustic systems, and given an adaptive–passive system which tunes in the presence of multi-tonal noise, the next step is to combine these two into a hybrid noise control system. As proven by Bode [10], feedback-based ANC must have frequency ranges of both noise attenuation and noise amplification. The adaptive–passive system, by contrast, achieves noise attenuation over a narrow frequency band which is tunable. Therefore, by combining an adaptive–passive Helmholtz resonator with a feedback ANC system, the resonator can be used to attenuate noise in the frequency ranges where the ANC has poor performance.

The remainder of the paper is organized as follows. First, the design of the adaptive–passive system is described and validated with a simple noise source. Next, the controller design methodology is outlined, and some of its characteristics are discussed. Then the two are integrated and tested against more complex signals. During the design process, the interaction between the two subsystems is explicitly considered.

2. ADAPTIVE–PASSIVE NOISE CONTROL

Presented in this section is the development of the adaptive–passive noise control solution. A tunable Helmholtz resonator is chosen as the adaptive–passive element and is designed based on a lumped parameter model. The intelligence of the device is achieved by a robust tuning algorithm for adaptive–passive noise control. This proposed tuning algorithm enables the adaptive–passive Helmholtz resonator to tune in the presence of multiple tones.

2.1. HELMHOLTZ RESONATOR DESIGN

The natural frequency of a Helmholtz resonator based on a lumped parameter model is given by

$$2\pi f_n = \omega_n = c\sqrt{\frac{S}{L_{eff}V}}, \tag{1}$$

where S is the area of the neck (m^2), c the speed of sound (m/s), L_{eff} the effective length of the neck (m), f_n the natural frequency in Hz, ω_n the natural frequency in (rad/s), and V the volume of the resonator (m^3) [11]. To tune the resonator, one of these parameters must be controlled. In this study, the Helmholtz resonator parameter chosen for tuning is the resonator volume, V.

The variable volume Helmholtz resonator is realized by attaching a neck to a pneumatic air cylinder. A schematic of the adaptive–passive element is shown in Figure 1. The air cylinder piston rod is linked to a DC motor via a lead screw to accomplish resonator tuning. A linear potentiometer is attached to achieve position feedback. As the piston position is altered, the volume of the resonator changes, thereby changing the natural frequency. The usable frequency range of the resonator is $f_n \in [270, 790]$ Hz. The design parameters of the Helmholtz resonator are given in Table 1.

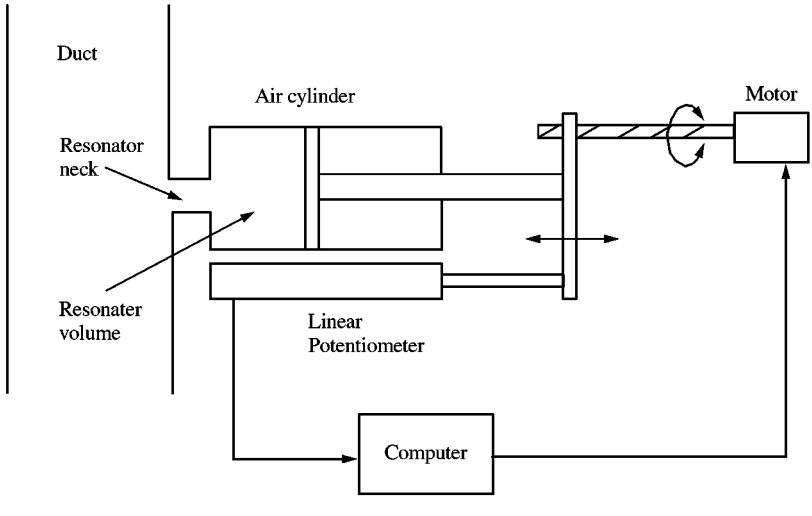

Figure 1. Schematic of the piston positioning system.

TABLE 1

The design parameters for the Helmholtz resonator

Neck	
Radius	1·3 cm
Length	7·0 cm
Body	
Radius	2·5 cm
Minimum length	0.63 cm
Maximum length	10 cm

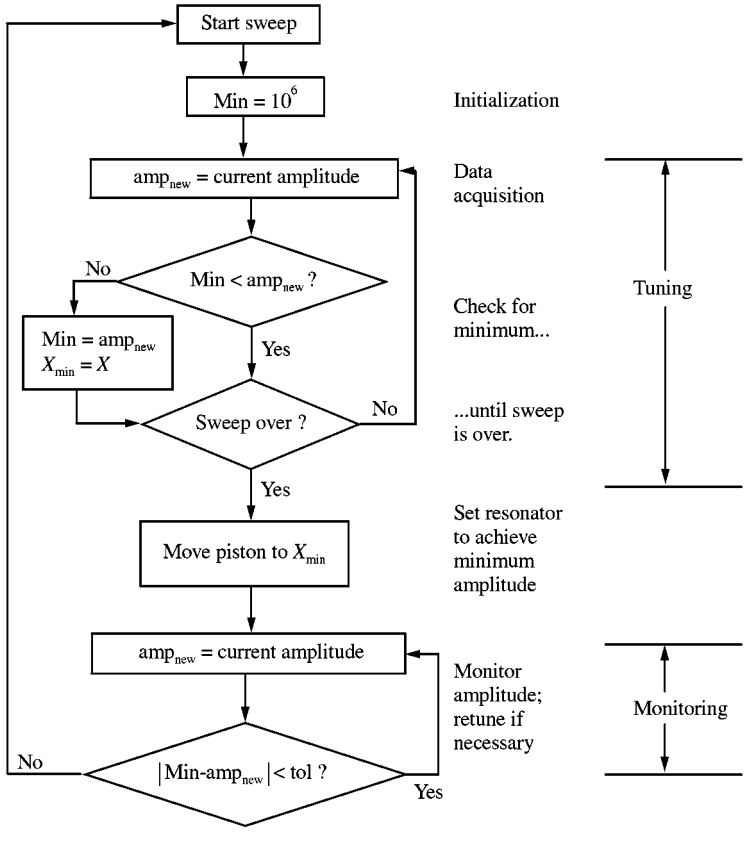

Figure 2. Flowchart of the tuning algorithm for the Helmholtz resonator.

2.2. ROBUST TUNING ALGORITHM

The proposed tuning algorithm is based on a global sweep over the resonator frequency range. The algorithm seeks to minimize the sound pressure level at the microphone by varying the Helmholtz resonator natural frequency. A flow chart of the algorithm is shown in Figure 2.

The algorithm has two stages: a tuning stage and a monitoring stage. During the tuning stage, the tuning algorithm seeks the optimal value for the resonator natural frequency by

sweeping through a preset range of natural frequencies. The piston position is swept by a feedback-based position control system. As the piston moves through the length of the cylinder, the corresponding amplitude of the microphone signal is monitored. Once the sweep is completed, the resonator is tuned to the piston position where the minimum amplitude occurred. During the monitoring stage, the tuning algorithm ensures that the sound pressure level in the duct remains acceptable. If the sound pressure level increases significantly, then the Helmholtz resonator is retuned. Thus, despite changes in the disturbance frequency content, the optimal tuning is maintained.

The amplitude of the microphone signal is determined using a circuit similar to that proposed by deBedout *et al.* [4]. In particular, the AC microphone signal is rectified and then low-pass filtered to produce a DC signal. Simple logic is then used to identify the minimum DC value and store the corresponding resonator position.

The goal of this global search is to minimize the steady state output noise level from the duct. Therefore, the transients introduced in the microphone signal due to Helmholtz resonator tuning (i.e., piston movement) must be negligible. This condition translates into an allowable position sweep rate for piston movement [12]. Specifically, the piston movement must be slow in comparison to the setting time of the Helmholtz resonator dynamics. It can be shown that for this experimental set-up, the allowable piston sweep rate is upper bounded by

$$\dot{x}(t) < 0{\cdot}08 \text{ cm/s}, \tag{2}$$

where $\dot{x}(t)$ denotes the piston velocity [12]. In all tests, the sweep rate was held below 0·05 cm/s.

2.3. EXPERIMENTAL SET-UP

A schematic of the entire duct system is shown in Figure 3. The system consists of a 5 cm diameter PVC pipe with an open, unflanged termination at one end and a disturbance speaker at the other end. The overall pipe length is 81·3 cm and is divided into sections so

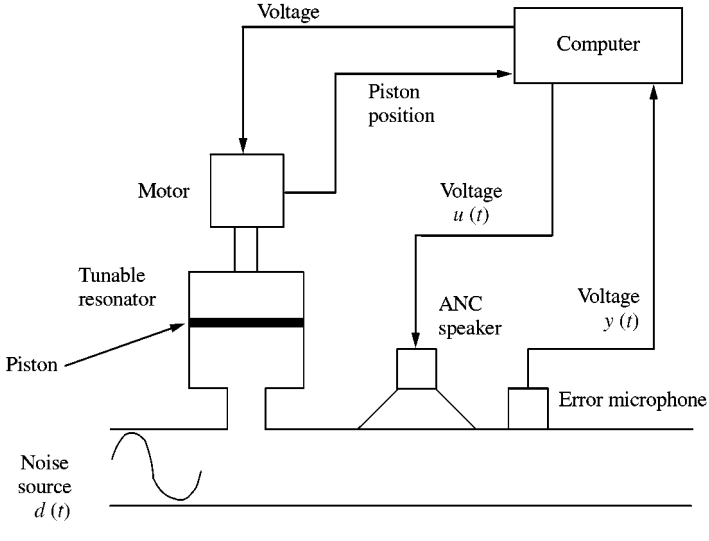

Figure 3. Schematic of the hybrid noise control system.

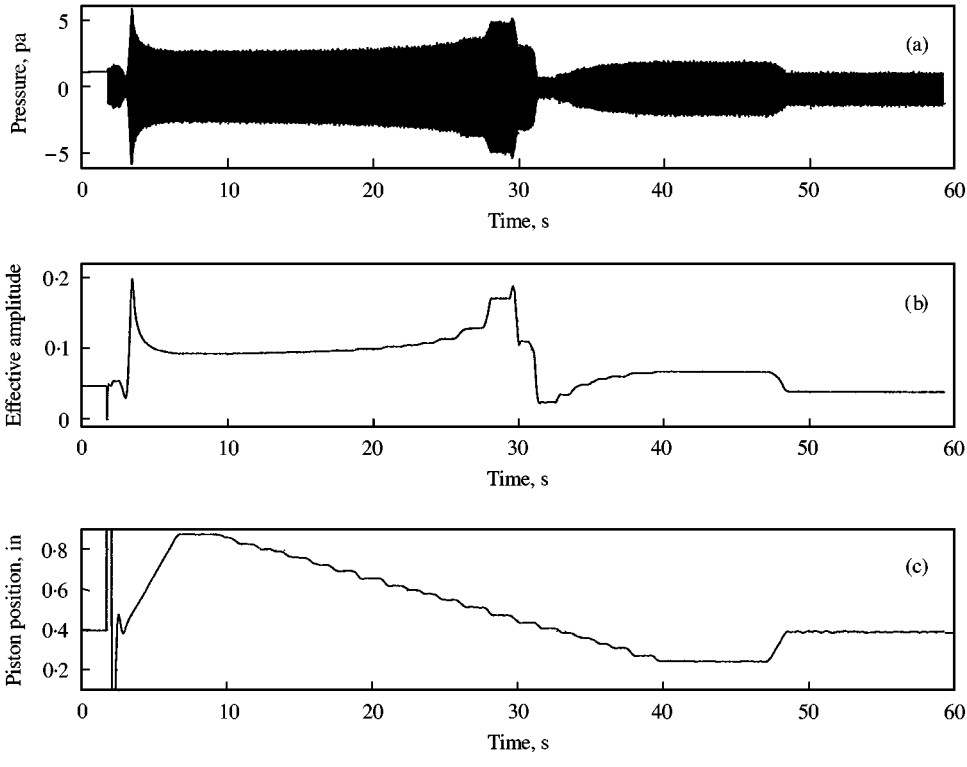

Figure 4. The system response to a tone at 700 Hz. (a) Time history of the pressure at the feedback microphone during tuning. (b) The output of the amplitude detector during tuning. (c) The piston position during tuning.

that the various elements can be inserted and removed. The feedback microphone, ANC speaker, and Helmholtz resonator are located 9·5, 30·5 and 57·8 cm, respectively, from the open end of the duct. The fact that the feedback microphone and loudspeaker are non-collocated introduces a time delay into the system. This time delay has important implications for the feedback controller. While the non-collocated configuration is not typical of the tight-coupled monopole, it could appear due to space limitations or environmental considerations during implementation.

Both the disturbance speaker and the ANC speaker are Realistic 4 in woofers housed in a section of duct with a diameter of 10·4 cm. The housing is 5·0 cm and connected to the main duct. The signal to each speaker is amplified by a QSC 2 channel, 70 W, stereo amplifier. The gain of the amplifier is set to unity. The feedback microphone is a 0·5 in B&K 4130 condenser microphone connected to a B&K 2642 preamplifier and 2810 power supply. The disturbance waveforms are generated on a Tektronix 2630 Personal Fourier analyzer. The Tektronix is also used to measure the frequency response functions.

2.4. VALIDATION OF ROBUST TUNING ALGORITHM

The adaptive–passive algorithm was validated in the presence of a pure tone at 700 Hz. The transient performance of the tuning algorithm is shown in Figure 4. The output of the amplitude detector (middle figure) has the same qualitative behavior as the actual pressure signal from the microphone (top figure), demonstrating the performance of the tuning

algorithm. The system does not quite attain the optimum performance due primarily to mechanical issues in the positioning system: backslash, deadbands, etc.

3. ROBUST FEEDBACK-BASED ACTIVE NOISE CONTROL

The proposed active noise controller design methodology is executed in the frequency domain. There are several important reasons motivating a frequency domain approach. First, dynamics of acoustic systems are naturally displayed in the frequency domain. Second, frequency domain methods transparently display the inherent trade-offs between closed-loop performance and controller bandwidth as identified by the Bode sensitivity integral [10]. Third, pure delays and non-propagating modes, inherent in acoustic systems, can be directly incorporated into the controller design process. Fourth, unrealistic assumptions on the duct, loudspeaker and microphone models can be completely avoided since controller design can be performed directly on measured frequency response functions. Finally, performance goals for active noise control systems are readily formulated in the frequency domain.

3.1. CONTROLLER DESIGN OBJECTIVE

A schematic of the acoustic system is shown in Figure 3. The signal $d(t)$ denotes the disturbance or noise source, $u(t)$ denotes the control effort (voltage input to the speaker). The system output is the sound pressure level measured in volts by the microphone and denoted as $y(t)$. The computer shown in Figure 3 realizes the feedback noise controller as well as the tuning algorithm for the Helmholtz resonator. The adjustable Helmholtz resonator and ANC speaker are also shown.

Shown in Figure 5 is a block diagram representation of the same system where all signals and system dynamics have been converted to the Laplace domain. The transfer function $P(s)$ denotes the system dynamics from $U(s)$ to $Y(s)$ which includes the speaker, duct,

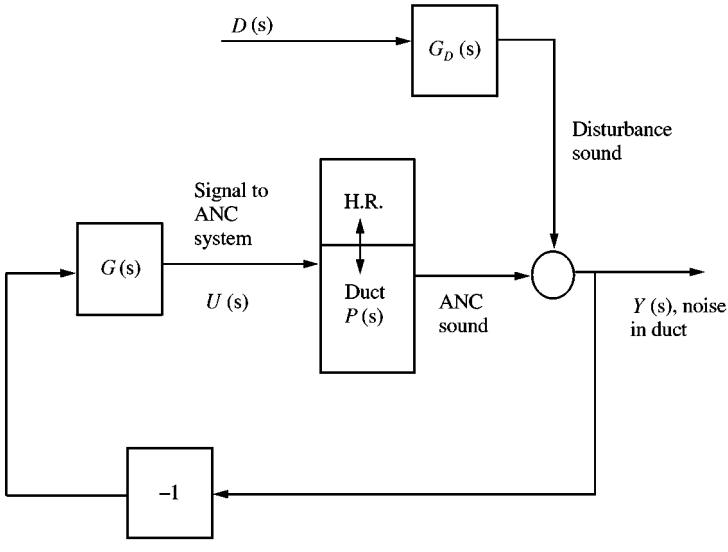

Figure 5. Block diagram of the active noise control system.

microphone and anti-aliasing filter. The feedback controller, $G(s)$, denotes the transfer function from the output (microphone voltage), to the control effort (speaker input voltage) The transfer function from $D(s)$ to $Y(s)$ is denoted by $G_D(s)$. Both $P(s)$ and G_D(s) change when the Helmholtz resonator is tuned. Therefore, the parameter α will be introduced in the following development to denote the parametric changes in the duct dynamics due to different Helmholtz resonator settings.

Without control, the microphone output is

$$Y(s, \alpha) = G_D(s, \alpha) D(s), \tag{3}$$

while with closed-loop control the microphone output is

$$Y(s, \alpha) = \frac{1}{1 + L(s, \alpha)} G_D(s, \alpha) D(s), \tag{4}$$

where $L(s, \alpha) = G(s)P(s, \alpha)$ is the so-called open-loop transfer function.

The ANC objective is to reduce the transmission of $D(s)$ to $Y(s, \alpha)$ over the frequencies of interest. Dividing equation (4) by equation (3) gives $1/(1 + L(s, \alpha))$, the ratio of closed-loop to open-loop performance. The term $1/(1 + L(s, \alpha))$ is the so-called closed-loop sensitivity transfer function and is denoted as $S(s, \alpha)$ [10]. The ANC problem can therefore be formulated as

$$\min_{\omega \in \Omega, G(j\omega) \in \mathscr{G}} \left| \frac{1}{1 + L(j\omega, \alpha)} \right| = \min_{\omega \in \Omega} |S(j\omega, \alpha)|, \tag{5}$$

where Ω is the set of frequencies where noise reduction is desired, $S(j\omega, \alpha)$ denotes the sensitivity function, $\mathscr{G}$ denotes all stabilizing controllers and the Laplace transforms have been converted into Fourier transforms by setting $s = j\omega$. To reduce the magnitude of $S(j\omega, \alpha)$ through the design of a stabilizing controller, $G(j\omega)$, the magnitude of $(1 + L(j\omega, \alpha))$ must be lower bounded. Thus, $|L(j\omega, \alpha)|$ is lower bounded. This conclusion agrees with the well-known result that high loop-gain corresponds to high noise attenuation.

3.2. CONNECTING OPEN-LOOP CHARACTERISTICS WITH CLOSED-LOOP PERFORMANCE

To design $G(j\omega)$ to reduce $|S(j\omega, \alpha)|$, a connection between open-loop frequency response characteristics and closed-loop performance must be made. Without loss of generality, the parameter α will be suppressed in the following development for the sake of clarity.

The mapping between open- and closed-loop frequency domain information is accomplished as follows. Let $L(j\omega) = a(\omega) + ib(\omega)$ and $|S(j\omega)| = |1 + L(j\omega)|^{-1} = C$ where C is a constant. It follows that

$$[1 + a(\omega)]^2 + b^2(\omega) = \frac{1}{C^2}. \tag{6}$$

Equation (6) represents a circle centered at $(-1, 0)$ in the $L(s)$ plane with radius of $1/C$. Thus, line of constant closed-loop sensitivity are circles in the $L(s)$ plane.

Commonly, frequency domain information is presented in Bode plots. While Bode plots effectively display frequency response information, this representation is not the most conducive for controller design. An alternative representation of frequency response

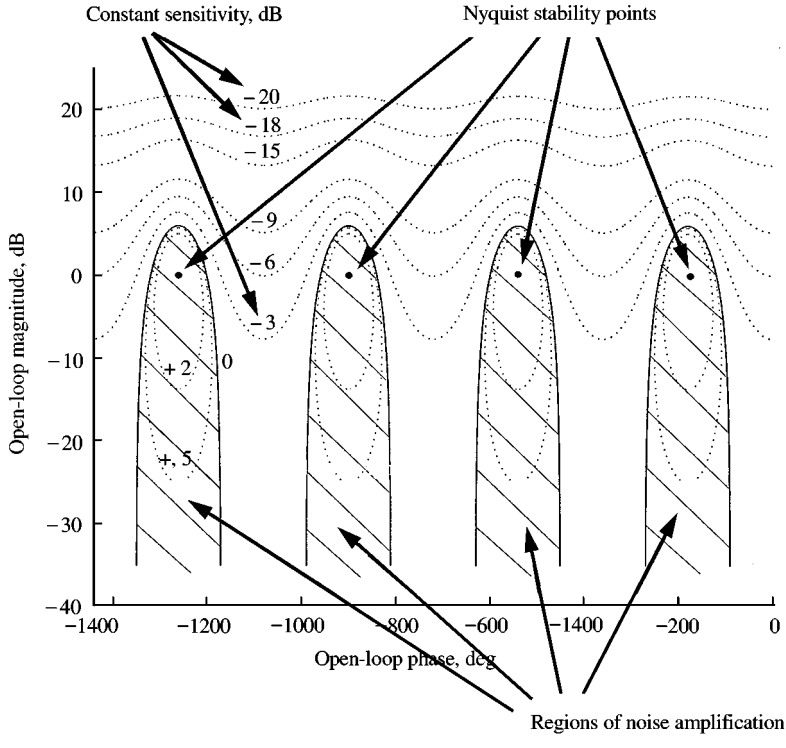

Figure 6. Sensitivity chart.

information is the open-loop gain-phase plane. In the gain-phase plane, the frequency response characteristics are plotted as the set of ordered pairs

$$\{\angle L(j\omega),\ 20\log_{10}|L(j\omega)|\}, \tag{7}$$

where $L(s)$ denotes the open-loop transfer function. When lines of closed-loop sensitivity are plotted in the open-loop gain-phase plane, the resulting figure is referred to as a sensitivity chart. A sensitivity chart is displayed in Figure 6.

The sensitivity chart is separated into regions of noise attenuation and regions of noise amplification by the 0 dB contour (Figure 6). Noise frequencies for which $L(j\omega)$ lies inside the 0 dB contour will be amplified by the closed-loop system. Similarly, noise frequencies for which $L(j\omega)$ lies outside the 0 dB contour will be attenuated by the closed-loop system. The controller design process focuses on placing frequencies of interest in regions of high attenuation while satisfying the Nyquist encirclement condition.

The sensitivity chart has been developed here from a robust control approach. Mangiante [13], however, derived a similar result based on acoustic arguments.

3.3. CLOSED-LOOP STABILITY AND THE NYQUIST ENCIRCLEMENT CONDITION

Closed-loop stability can be inferred from the open-loop frequency response via the Nyquist encirclement condition [14]. If $L(s)$ is stable, then the Nyquist encirclement condition guarantees closed-loop stability if $|L(j\omega)| < 1$ for the frequencies where $\angle L(j\omega) = k180^\circ$, where k is an odd integer.

A general proof of the Nyquist encirclement condition requires results from the theory of complex variables. For the acoustic system here, however, an intuitive interpretation can be given. The negative feedback causes a phase change of 180° between the microphone and the input to $L(s)$. If the open-loop system has approximately zero phase lag at a frequency ω_{0°, that is, if $\angle L(j\omega_{0^\circ}) \approx -k180^\circ$, k even, then the total phase change for the signal is approximately 180°, destructive interference will occur, and high gain leads to high attenuation. If, however, the open-loop system has approximately -180° lag at a frequency ω_{180°, that is $\angle L(j\omega_{180^\circ}) \approx k180^\circ$, k odd, then the total phase change for the feedback signal is approximately 0°, leading to constructive interference. At these frequencies, the feedback loop must attenuate the signal,

$$|L(j\omega_{180^\circ})| < 1, \tag{8}$$

to maintain stability.

3.4. CONTROLLER DESIGN PROCESS: LOOP SHAPING

Most studies centered on the tight-coupled monopole and similar devices focus on the acoustic interpretation of the solution [8, 9, 15]. Typically, the controller is simply an inverting amplifier, commonly referred to as a proportional feedback controller. In multi-resonant systems, strict proportional feedback control becomes unstable or has poor performance. To improve the performance of proportional control, the higher frequency resonances must be attenuated using passive means such as acoustic damping material. In addition, time delays tend to destabilize proportional feedback systems thereby limiting closed-loop performance to the low-frequency range. Thus, although proportional control facilitates an acoustic interpretation, the full performance potential of feedback-based noise control is not necessarily achieved. In particular, proportional control cannot achieve robust performance in uncertain, multi-resonant, time-delayed systems, such as the duct system presented here. An alternative set of design tools is required.

A controller design process called loop shaping possesses the requisite flexibility for effective ANC design [10, 16]. Loop shaping is initiated by displaying the frequency response function (measured in this case) of the acoustic system on a sensitivity chart. The design goal is to choose the controller, $G(j\omega)$, such that the compensated open-loop frequency response function, $L(j\omega, \alpha) = G(j\omega)P(j\omega, \alpha)$, lies in regions of noise attenuation while satisfying the Nyquist encirclement condition.

Using a loop-shaping approach extends the impact of feedback control to higher frequencies ranges, allowing multiple resonant peaks to be attenuated. By manipulating the open-loop gain-phase characteristics, $L(j\omega, \alpha) = G(j\omega)P(j\omega, \alpha)$, via the controller frequency response, $G(j\omega)$, resonances in the original acoustic system can be shifted into the regions of performance. Far from destabilizing the system (as in the case of proportional control), resonant peaks *can be used to achieve performance*.

3.5. EXAMPLE DESIGN USING THE SENSITIVITY CHART

To illustrate the ANC system and to illustrate its characteristics, a feedback controller is designed for a single setting of the Helmholtz resonator. The qualitative design goal is to reduce the magnitude of the first resonant peak while maintaining stability despite high-frequency resonances. The Helmholtz resonator is set to have a natural frequency of 690 Hz. Therefore, in this section, the parameter α will be suppressed. The experimental

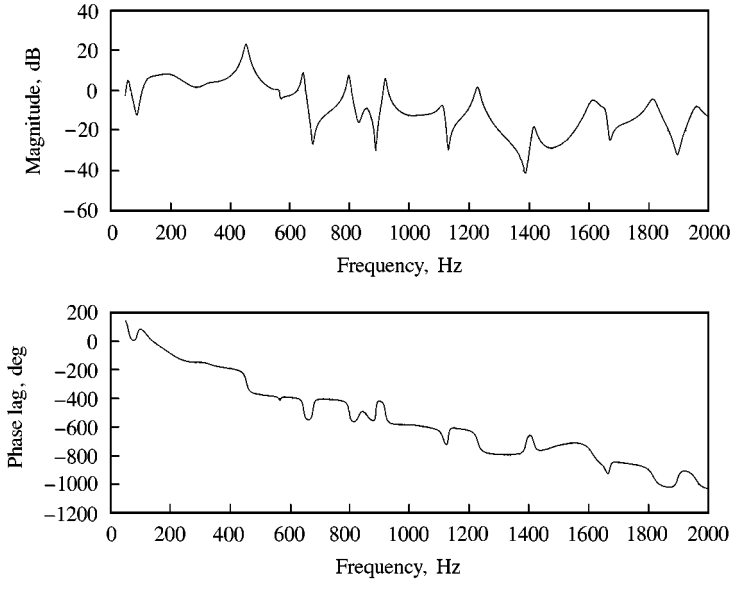

Figure 7. Frequency response from the control speaker to the error microphone.

system is similar to that described in section 2.3, with the only difference being that a different disturbance loudspeaker is used.

The configuration of the experimental testbed in this project presents two key challenges during controller design. First, the microphone and loudspeaker are not collocated. Hence, the system contains a significant time delay. Second, the system possesses significant uncertainty due to the tuning of the adaptive-passive Helmholtz resonator. Consideration of the uncertainty due to the adaptive–passive system is deferred to section 4, but the effects of non-collocation are included in this section.

To begin the controller design process, the frequency response function from $U(j\omega)$ to $Y(j\omega)$, $P(j\omega)$ is measured. This frequency response function is shown in Figure 7, and it is plotted on a sensitivity chart in Figure 8. Once the frequency response function is identified, the next step is to design a controller such that the resonances of $L(j\omega) = G(j\omega)P(j\omega)$ are positioned between the stability points on the sensitivity chart.

To understand the design process fully, it is crucial to understand the information presented in the sensitivity chart. Because low frequencies have low phase lag and high frequencies tend to have higher phase lag, frequency will increase from right to left on a sensitivity chart. The increase is not, however, monotonic. Another feature to notice in Figure 7 is the large phase lag. Two factors cause this. First, the time delay creates a phase lag linear with frequency, and second, the frequency response indicates the system dynamics has more poles than zeros. The large phase lag means that on the sensitivity chart the frequency response function will extend across a wide phase range. The first resonant peak, near 460 Hz, is prominent in both Figures 7 and 8. Finally, Figure 8 contains several large loops. Such loops are formed by closely spaced sets of lightly damped poles and zeros. For example, the resonance at about 650 Hz is followed by an antiresonance at 690 Hz. These cause the magnitude and phase to undergo large changes over a frequency range of 50 Hz.

The data in Figure 8 display the information needed for controller design, the most immediate issue being closed-loop stability. For example, the amplitude condition of $|L(j\omega)| < 1$ is not satisfied at the critical point located at -180° near a frequency of 300 Hz.

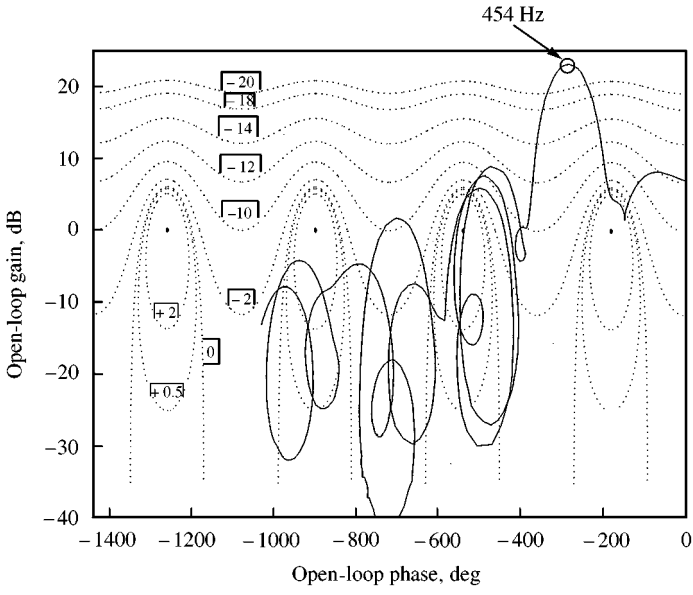

Figure 8. Frequency response from the control speaker to the error microphone plotted on a sensitivity chart.

There is another violation of the Nyquist encirclement condition at -540°. Several options exist to stabilize the feedback system. One solution is to reduce the open-loop DC gain of the feedback system until the frequency response function passes beneath all the Nyquist stability points. This is the typical method for tight-coupled monopoles. A second option, followed here, is to reshape the open-loop frequency response. In particular, the phase lag of the controller will be such that the resonant peaks of $L(j\omega) = G(j\omega)P(j\omega)$ are centered between the stability points. Hence, the high-open-loop gain characteristics of $P(j\omega)$ are employed to achieve noise control. As a result, the Nyquist encirclement condition will be satisfied.

Summarizing this discussion, the specific design goals for this problem are as follows.

- Stabilize the system by adjusting the magnitude to be less than unity (0 dB) at frequencies with phase lag of $\angle L(j\omega) = k = 180^\circ$, k odd (stability).
- Position the resonant peak at 460 Hz between the stability points with the highest gain consistent with stability (performance).
- Do not cause more than 2 dB amplification at any frequency (performance/robust stability).
- Attenuate higher frequency resonances (robust stability).

These goals are satisfied with the second order controller

$$G(s) = \frac{0{\cdot}0562}{(s/2\pi 470)^2 + 2 \times 0{\cdot}18 s/2\pi 470 + 1}. \tag{9}$$

The compensated frequency response function is shown in Figure 9. The phase lag of $G(j\omega)$ places the system resonance between the stability points, and the high-frequency roll off of $G(j\omega)$ attenuates all higher resonances of $L(j\omega)$. Being lightly damped, the controller, $G(j\omega)$, adds gain at 470 Hz, increasing performance. Finally, the overall gain of the controller is set

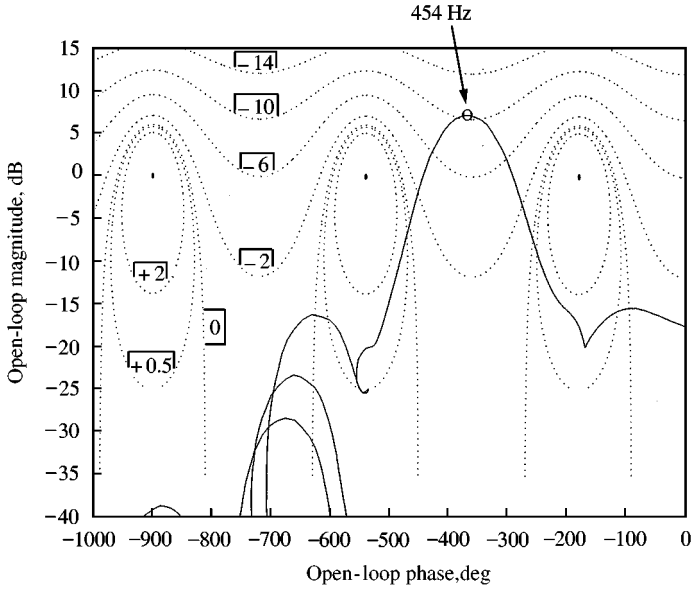

Figure 9. The open-loop frequency response function, $L(j\omega) = G(j\omega)P(j\omega)$.

to keep $L(j\omega)$ outside the $+2$ dB sensitivity contour. Avoiding the $+2$ dB contour ensures robust stability and closed-loop performance.

3.6. IMPLEMENTATION AND PERFORMANCE OF THE ANC SYSTEM

While this controller can be constructed with low-cost capacitors, resistors, and op-amps [17], it was implemented digitally for convenience during testing. The controller was converted to the discrete domain with a sample frequency of 35 000 Hz. An anti-aliasing filter was set to achieve 40 dB attenuation at 17 000 Hz. The frequency response from the disturbance to the error microphone was measured with the ANC turned on and turned off. The data are displayed in Figure 10.

The data agree with the predicted performance. The resonant peak at 460 Hz is significantly attenuated in the closed-loop system. The predicted maximum attenuation is slightly more than 10 dB. The closed-loop system has about 2 dB amplification from about 200 Hz to about 400 Hz and in the resonant peak at about 550 Hz. The frequency ranges of amplification can be seen in Figure 9 and are consistent with the implications of the Bode sensitivity integral.

In a practical system, attenuating the resonance at 550 Hz would be an important goal. This resonance does not, however, appear in the frequency response function $P(j\omega)$. Achieving high gain at 550 Hz, $|L(j2\pi550)| > 1$, would require high gain in the controller, $|G(j2\pi550)| > |P(j2\pi550)|^{-1}$, and thus large actuator effort. Another solution would be to change the location of the control speaker such that the resonances to be attenuated appear in $P(j\omega)$. In either of these cases, it may prove difficult to create the proper phasing since the peaks are so closely spaced in frequency.

To establish the performance of the ANC system away from the error microphone, the frequency response function from the disturbance to various points was measured with and without control. Points were selected at 5 cm increments beginning 5 cm from the open end

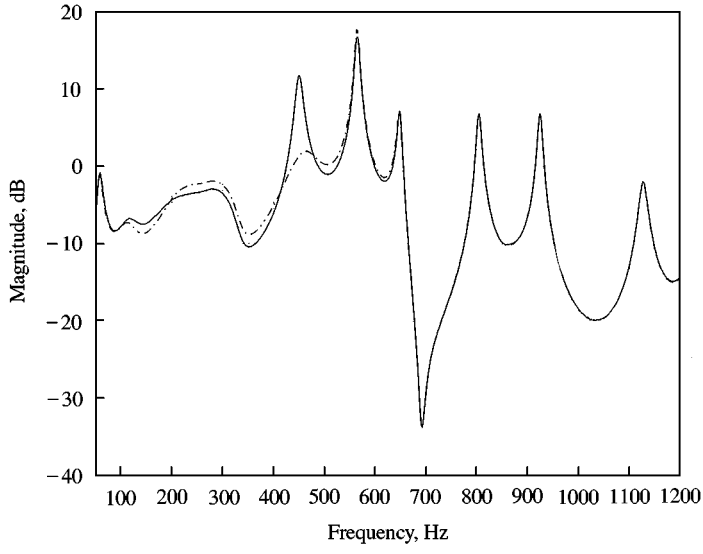

Figure 10. Frequency response from disturbance to error microphone with (– · – ·) and without (- - -) control.

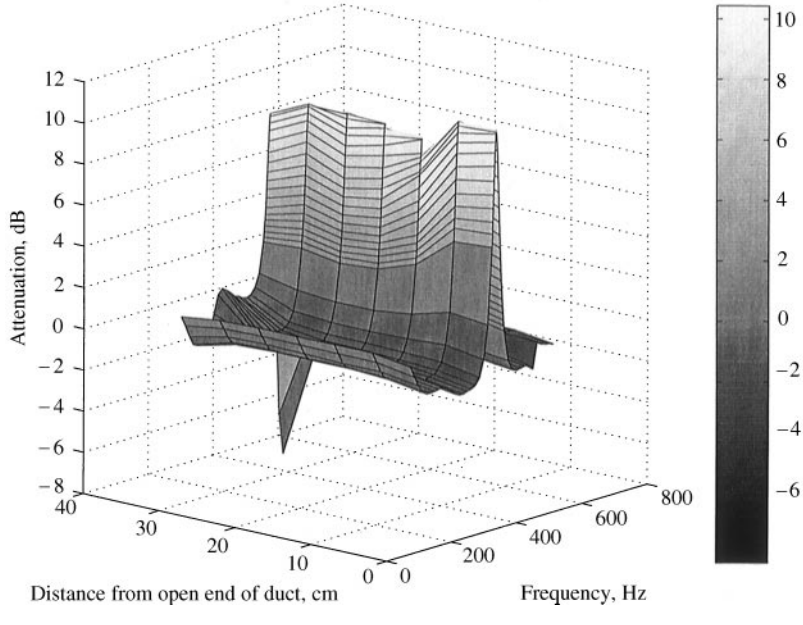

Figure 11. Attenuation as a function of space and frequency. The ANC speaker is located 30 cm from the open end of the duct, and the feedback microphone is located 9·5 cm from the open end.

of the duct. The attenuation caused by the ANC system is displayed in Figure 11 as a function of location and frequency. The surface displayed in Figure 11 is relatively flat with a ridge at about 460 Hz extending from about 40 cm to the end of the duct. The sensitivity chart predicted 10 dB attenuation at the microphone, and the ridge is 10 dB high at 10 cm and 5 cm. These data show that the attenuation caused by the ANC is not restricted to a single point, but exists at all points downstream of the speaker.

4. APPLICATION OF HYBRID NOISE CONTROL

In this section, the complete hybrid system is presented. A feedback active noise controller is designed to complement the adaptive–passive Helmholtz resonator. The adaptive–passive system provides noise attenuation at frequencies where the ANC system cannot. The design of each subsystem explicitly includes the interaction between the two separate subsystems. Since the Helmholtz resonator is tuned by the adaptive–passive algorithm, the parameter α will be used in this section. The experimental system used here is identical to that used in section 2.

4.1. ADAPTIVE–PASSIVE HELMHOLTZ RESONATOR

The gain $|P(j\omega, \alpha_0)|$, where α_0 corresponds to the resonator removed from the system, is above 15 dB from about 100 to 650 Hz (Figure 12). Once the system is stabilized, the high gain in this frequency range will lead to significant noise attenuation. From about 650 to 850 Hz, however, the gain of the frequency response function is lower. To achieve noise attenuation in this frequency range, the active noise control system would require considerable gain from the controller while adjusting the phase to maintain closed-loop stability. Rather than use control effort from the ANC system over this frequency range, the adaptive–passive Helmholtz resonator is used to reduce the noise in the duct. If the Helmholtz resonator tunes in this range, then noise attenuation is not required from the ANC. To limit the tuning strategy of the Helmholtz resonator to this frequency range, the noise signal used for tuning is bandpass filtered to attenuate frequencies outside this range.

4.2. ACTIVE NOISE CONTROLLER DESIGN

To begin the controller design process, the dynamics of the acoustic system are represented in the frequency domain. Three distinct cases are considered, one with the Helmholtz resonator removed and two with the Helmholtz resonator set at the natural

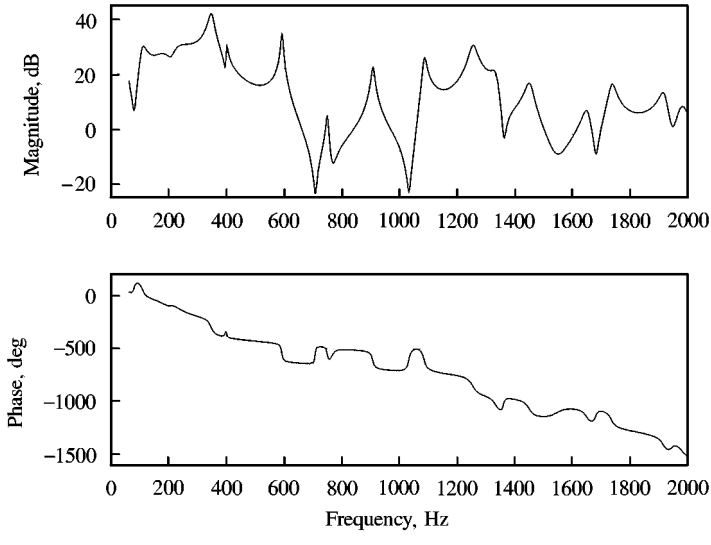

Figure 12. Frequency responses from the control speaker to the disturbance microphone, Helmholtz resonator removed.

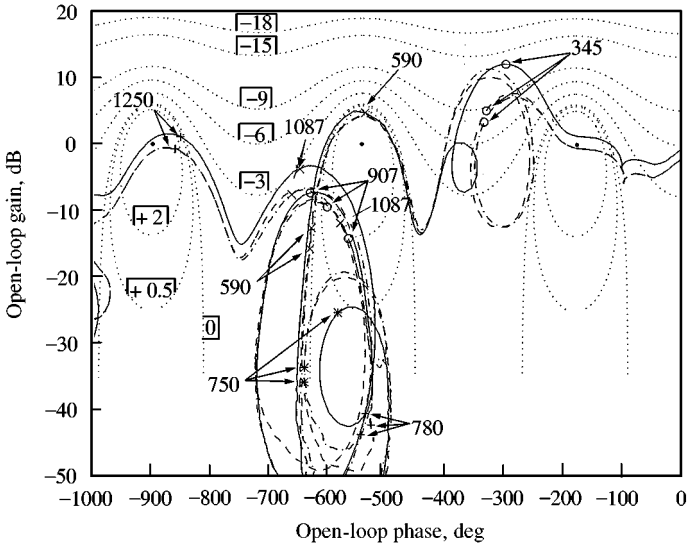

Figure 13. Frequency responses from the control speaker to the disturbance microphone for several different settings of the Helmholtz resonator. No resonator (——), resonator set to 690 Hz (– · – · –), resonator set to 790 Hz (- - -).

frequencies of 690 and 790 Hz. These three cases represent a few of the various possible system frequency responses. All three acoustic systems are used to design one fixed coefficient controller.

Once the frequency response functions are identified, the next step is to design a controller such that the resonances of $L(j\omega, \alpha) = G(j\omega)P(j\omega, \alpha)$ are positioned between the stability points on the sensitivity chart. Figure 13 shows the three open-loop measured frequency response functions in the gain-phase plane with a controller beginning as $G(s) = 0{\cdot}032$. Three resonances are controlled: 345, 590, and 1250 Hz. The restriction of less than 2 dB amplification in the closed loop is removed. The design goal is to achieve the maximum attenuation at these three frequencies subject to robust stability margins.

To shape $L(j\omega, \alpha)$ such that the main resonances are between the stability points while not changing open-loop magnitude, an all-pass filter comprised of complex poles and zeros is used. The general form of the filter transfer function is given by

$$\frac{(s/2\pi f_n)^2 - 2 \times \zeta s/2\pi f_n + 1}{(s/2\pi f_n)^2 + 2 \times \zeta s/2\pi f_n + 1}.$$

This filter has unity magnitude for all frequencies, but has considerable phase lag. At a frequency of f_n, the filter adds 180° of phase lag, and at high frequencies 360° of lag are contributed. Choosing $f_n = 850$ Hz, $\zeta = 0{\cdot}4$, the phase characteristics of $L(j\omega)$ are changed at frequencies above about 160 Hz while maintaining the same gain characteristics.

Each of the three main resonances are addressed individually. To properly shape the phase at the resonance of 590 Hz, as well as increase its magnitude, a pair of lightly damped poles, $f_n = 590$ Hz, $\zeta = 0{\cdot}15$, are included. The gain of $L(j\omega, \alpha)$ at 1250 Hz is increased and the resonant peak centered between the stability points by adding two pairs of poles, one at $f_n = 1275$ Hz, $\zeta = 0{\cdot}2$ and the other at $f_n = 1275$ Hz, $\zeta = 0{\cdot}18$. To avoid the sensitivity amplification region at low frequencies, a notch filter is used. The notch filter consists of complex zeros located at $f_n = 210$ Hz, $\zeta = 0{\cdot}25$ and a pair of complex poles at $f_n = 210$ Hz,

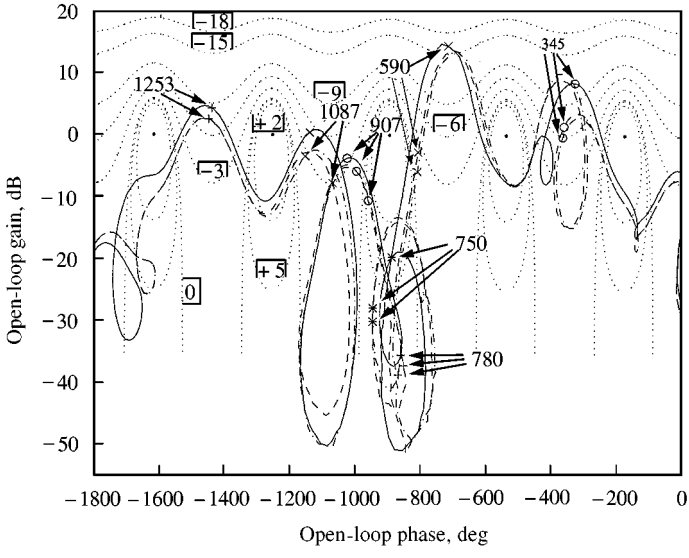

Figure 14. Sensitivity chart of the compensated open-loop frequency response functions. No resonator (——), resonator set to 690 Hz (–·–·–), resonator set to 790 Hz (- - -).

$\zeta = 1$, Finally, the DC gain of the controller is re-adjusted to 0·025 to satisfy stability margins while giving closed-loop performance. The compensated open-loop frequency responses, $L(j\omega, \alpha)$, are shown in Figure 14. The resulting controller is

$$G(s) = 0{\cdot}025\left(\frac{(s/2\pi 850)^2 - 2\times 0{\cdot}4s/2\pi 850 + 1}{(s/2\pi 850)^2 + 2\times 0{\cdot}4s/2\pi 850 + 1}\right)\left(\frac{1}{(s/2\pi 590)^2 + 2\times 0{\cdot}15s/2\pi 590 + 1}\right)$$
$$\left(\frac{1}{(s/2\pi 1275)^2 + 2\times 0{\cdot}2s/2\pi 1275 + 1}\right)\left(\frac{1}{(s/2\pi 1275)^2 + 2\times 0{\cdot}18s/2\pi 1275 + 1}\right)$$
$$\left(\frac{(s/2\pi 210)^2 + 2\times 0{\cdot}25s/2\pi 210 + 1}{(s/2\pi 210)^2 + 2\times 1s/2\pi 210 + 1}\right). \tag{10}$$

For implementation equation (10) is mapped into the discrete domain with sampling frequency of 20 000 Hz. The frequency response of the discretized controller agrees with the frequency response of the continuous controller up to 1600 Hz. Alternatively, an analog circuit with the appropriate transfer function could have been created [17].

4.3. PERFORMANCE OF THE HYBRID SYSTEM

A signal consisting of two dominant tones, one at 590 Hz and one at 750 Hz, was generated to illustrate the performance of the hybrid noise control system. Four different scenarios were tested to evaluate the performance: (1) Helmholtz resonator removed and the ANC inactive; (2) Helmholtz resonator tuned by the adaptive–passive tuning algorithm and the ANC inactive; (3) Helmholtz resonator tuned and the ANC active; and (4) Helmholtz resonator removed from the system and the ANC active. The results are shown in Table 2. These same four scenarios were performed with a disturbance consisting of four tones: 340, 590, 750, and 1250 Hz. The results of these are summarized in Table 3.

TABLE 2

Effect of the hybrid system on a two-tone noise

	ANC (dB)	Adaptive–passive (dB)	Hybrid (dB)
590 Hz	− 15·5	− 16·5	− 18·0
750 Hz	+ 1	− 16·0	− 15·5

TABLE 3

Effect of the hybrid system on a four-tone noise

	ANC (dB)	Adaptive–passive (dB)	Hybrid (dB)
340 Hz	− 9·5	+ 0·5	− 7·0
590 Hz	− 15·0	− 16·5	− 17·5
750 Hz	+ 1	− 9·0	− 8·5
1250 Hz	− 8·5	+ 3	− 5

The results show that the adaptive–passive system does not isolate any single tone. Rather, the adaptive–passive system minimizes the overall band-pass filtered signal. Thus, the system tunes the Helmholtz resonator to a setting between 590 and 750 Hz. At this setting each tone is attenuated moderately (9 and 16 dB) instead of one tone being attenuated drastically (35 dB).

The active noise control results agree with the prediction obtained from the sensitivity chart. When the Helmholtz resonator is removed, the point $L(\mathrm{j}2\pi 590, \alpha)$ lies slightly above the -15 dB sensitivity contour in Figure 14. However, when the Helmholtz resonator is included and tuned in the range 690–780 Hz, the point $L(\mathrm{j}2\pi 590, \alpha)$ shifts below the -3 dB contour in Figure 14. The experimental results were 15·5 and 1·5 dB attenuation respectively.

As shown in Figure 14, the frequency response passes through several regions of noise amplification. While the original resonant peaks are attenuated, amplification is caused at other frequencies. This unavoidable trade-off in an inherent characteristic of feedback control systems and is quantified by the Bode sensitivity integral [10].

Although the resonant peaks of $L(\mathrm{j}\omega, \alpha)$ remain between the stability points for these resonator settings, the amplitude peaks do not correspond to the same frequencies. Thus, although the ANC is robustly stable and always attenuates noise at the frequencies of the resonant peaks, the performance at specific frequencies changes as the resonator tunes. Further, while the amplitude peaks of $L(\mathrm{j}\omega, \alpha)$ remain in regions of noise attenuation, the resonances at 590 and 345 Hz change phase slightly for different resonator settings.

5. CONCLUSIONS

Presented in this manuscript is a hybrid noise control system. First, a tuning strategy for adaptive–passive systems is discussed. Previous studies have been limited to tonal applications. The tuning algorithm proposed allows the adaptive–passive system to tune in the presence of multiple tones. This strategy attempts to minimize the sound pressure level

downstream of the adaptive–passive device. A bandpass filter weights one frequency range heavily, effectively limiting the system to that range.

Next, the development of a controller design methodology for feedback ANC which includes the tight-coupled monopole as a special case is presented. The methodology, based on concepts from the robust control literature, uses loop shaping on a sensitivity chart to design a controller that provides noise attenuation at the microphone. Features such as time delays, variations in the plant dynamics, and non-propagating resonances can be easily handled with this methodology. The resulting controllers can be implemented using low-cost analog electronics, in contrast to the hardware requirements of adaptive feedforward schemes. Stability can be guaranteed *a priori* given bounds on the plant frequency response function. An example controller is designed and implemented in a duct. The ANC achieves attenuation at all points downstream of the speaker, with the design value of attenuation occurring at points downstream of the microphone location. The maximum attenuation changes as a function of location in the duct. The exact nature of this dependence on location is not clear and indicates an interesting topic for further study.

A hybrid noise control system is implemented and verified for several noise signals. A feedback controller is designed accounting for the uncertainty due to the adaptive–passive Helmholtz resonator. The adaptive–passive system is used to attenuate noise in a frequency range where the feedback system is ineffective. The feedback controller maintained performance despite the variations associated with the resonator position. The system was tested against noise consisting of several tones.

Finally, extensions to broadband noise should be immediate. The tuning algorithm for the adaptive–passive system does not make any assumptions about the spectrum of the noise since it performs a global search. Similarly, by the principle of superposition, the ANC system will perform as predicted by the sensitivity chart no matter what type of noise is applied to the system.

ACKNOWLEDGMENT

The authors thank Professor J. Stuart Bolton for his insights and suggestions on this project.

REFERENCES

1. Hiroshi Matsuhisa, Baosheng Ren and Susumu Sato 1992 *JSME International Journal* **35**, 223–228. Semiactive control of duct noise by a volume-variable resonator.
2. J. S. Lamancusa 1987 *Proceedings of Noise-Con* 87, 313–318. An actively tuned, passive muffler system for engine silencing, State College, PA, U.S.A.
3. R. J. Bernhard 1994 *Proceedings of Noise-Con* 94, 421–428, The state of the art in active–passive noise control, Ft. Lauderdale, FL, U.S.A.
4. J. M. DeBedout, M. A. Franchek, R. J. Bernhard and L. Mongeau 1997 *Journal of Sound and Vibration* **202**, 109–123. Adaptive–Passive noise control with self-tuning Helmholtz resonators.
5. G. Koopmann and W. Neise 1982 *Journal of Sound and Vibration* **82**, 17–27. The use of resonators to silence centrifugal blowers.
6. P. Krause, H. Weltens and S. M. Hutchins February 1993 *Automotive Engineering* **101**, 13–16. Advanced exhaust silencing.
7. M. A. Franchek, M. W. Ryan and R. J. Bernhard 1995 *Journal of Sound and Vibration* **189**, 565–585. Adaptive passive vibration control.
8. M. C. J. Trinder and P. A. Nelson 1993 *Journal of Sound and Vibration* **89**, 95–105. Active noise control in finite length ducts.

9. W. K. HONG, Kh. EGHTESADI and H. G. LEVENTHALL 1987 *Journal of the Acoustical Society of America* **81**, 376–388. The tight-coupled monopole (TCM) and tight-coupled tandem (TCT) attenuators: theoretical aspects and experimental attenuation in an air duct.
10. H. W. BODE 1945 *Network Analysis and Feedback Amplifier Design*. New York: D. Van Nostrand Company, Inc.
11. L. E. KINSLER, A. R. FREY, A. B. COPPENS and J. V. SANDERS 1982 *Fundamentals of Acoustics*. New York: John Wiley & Sons, third edition.
12. T. KOSTEK 1998 *Masters Thesis, Purdue University*, Hybrid noise control in ducts.
13. G. A. MANGIANTE 1977 *Journal of the Acoustical Society of America* **61**, 1516–1523. Active sound absorption.
14. KATSUHIKO OGATA 1990 *Modern Control Engineering*. Englewood Cliffs, NJ: Prentice-Hall.
15. Kh. EGHTESADI and H. G. LEVENTHALL 1983 *Journal of Sound and Vibration* **91**, 11–19. A study of *n*-source attenuator arrays for noise in ducts.
16. ISAAC HOROWITZ 1993 *Quantitative Feedback Design Theory, QFT*. Boulder, CO: QFT Publications.
17. DONALD CHRISTIANSEN 1996 *Electronics Engineers' Handbook*. New York: McGraw-Hill, fourth edition.